






## Article

# Sustainable Near-Infrared Reflective Blue Pigments: Recycled Aluminum from Can Seals for Cobalt Aluminates in Cool Coatings

Dienifer F. L. Horsth <sup>1,2,\*</sup> , Julia de O. Primo <sup>2</sup> , Fauze J. Anaissi <sup>2,\*</sup> , Polona Umek <sup>3</sup>  and Carla Bittencourt <sup>1</sup> 

<sup>1</sup> Chimie des Interactions Plasma-Surface (ChIPS), University of Mons, 7000 Mons, Belgium; carla.bittencourt@umons.ac.be

<sup>2</sup> Chemistry Department, Universidade Estadual do Centro-Oeste, Guarapuava 85040-167, Brazil; juliadeoliveira@unicentro.edu.br

<sup>3</sup> Solid State Physics Department, Jožef Stefan Institute, 1000 Ljubljana, Slovenia; polona.umek@ijs.si

\* Correspondence: dhorsth@unicentro.edu.br (D.F.L.H.); anaissi@unicentro.br (F.J.A.)

**Abstract:** Inorganic cool pigments are widely used as cooling agents in residential coatings due to their ability to achieve near-infrared reflectance. These coatings can be designed to exhibit a variety of colors independent of their reflectivity and absorption properties. Recent studies have highlighted the development of novel near-infrared (NIR) blue pigments, with an increasing emphasis on environmentally sustainable options that demonstrate high NIR reflectivity. This trend highlights the importance of creating novel and eco-friendly NIR reflective blue pigments. This study presents the synthesis of cobalt aluminates with varying concentrations of coloring ions ( $\text{Co}^{2+}$ ), achieved through the recycling of aluminum can seals via chemical precipitation. The formation of the spinel phase was confirmed through X-ray diffraction (XRD), and a colorimetric analysis was performed in the CIE L\*a\*b\* color space. The synthesized pigments exhibited high near-infrared solar reflectance, with R% values ranging from 34 to 54%, indicating their potential as energy-efficient color pigments for use in coatings.



**Citation:** Horsth, D.F.L.; Primo, J.d.O.; Anaissi, F.J.; Umek, P.; Bittencourt, C. Sustainable Near-Infrared Reflective Blue Pigments: Recycled Aluminum from Can Seals for Cobalt Aluminates in Cool Coatings. *Colorants* **2024**, *3*, 253–262. <https://doi.org/10.3390/colorants3040017>

Academic Editor: Anthony Harriman

Received: 15 September 2024

Revised: 8 October 2024

Accepted: 10 October 2024

Published: 11 October 2024



**Copyright:** © 2024 by the authors. Licensee MDPI, Basel, Switzerland. This article is an open access article distributed under the terms and conditions of the Creative Commons Attribution (CC BY) license (<https://creativecommons.org/licenses/by/4.0/>).

**Keywords:** recycled metallic aluminum; near-infrared reflection; circular economy

## 1. Introduction

Cobalt blue, also referred to as Thénard blue, is an inorganic pigment defined by its chemical composition of  $\text{CoAl}_2\text{O}_4$ , which categorizes it as a cobalt aluminate. It was first synthesized by the French chemist Louis Jacques Thénard in 1799 during his investigations into cobalt compounds. The synthesis process involved a reaction between cobalt (2+) oxide and aluminum oxide at high temperatures. This reaction produced the Thénard cobalt blue pigment, a compound characterized by a crystalline structure known as spinel. The discovery of this pigment represents a significant advance in pigment chemistry, broadening the array of options available to artists, painters, and ceramic manufacturers [1]. Despite being synthesized over two centuries ago, the cobalt blue pigment remains in use in various industries due to its color intensity and stability. The spinel phase observed in this pigment guarantees color and thermal stability [1]. Beyond the protective covering capacity against weathering, the applications of inorganic pigments have recently expanded to include reductions in surface temperatures, a phenomenon attributed to their high near-infrared (NIR) reflectance [2,3]. Solar radiation spans a broad spectrum of wavelengths, ranging from approximately 295 nm to 2500 nm, comprising about 45% near-infrared (NIR) radiation (~700–2600 nm), 50% visible light (~400–700 nm), and 5% ultraviolet radiation (~300–400 nm) [4,5]. The highest concentration of solar energy occurs between 700 and 1200 nm, a range predominantly responsible for heat generation [6]. The implementation of materials with high solar reflectance in applications such as furniture, automobiles,

roofs, and other objects can effectively reduce heat gain [7]. Specifically, roofs with a high reflectance can maintain lower temperatures under sunlight, thereby reducing the demand for cooling energy in air-conditioned buildings and improving comfort in buildings lacking such systems [8,9]. Using cool pigments to lower internal temperature represents a viable strategy for enhancing solar reflectance [10,11]. Pigments with high reflectance in the NIR range have already been used in cold coatings applied to different surfaces, including walls, roofs, windows, facades, and vehicles [12]. These pigments can exhibit a range of colors due to their capacity to absorb and reflect ultraviolet–visible radiation (UV–vis) [5]. They are synthesized through various methodologies, including hydrothermal, combustion, coprecipitation, solid-state reaction, and sol–gel techniques [13–16].

This study presents a sustainable alternative for the synthesis of cobalt blue pigments through the recycling of metallic aluminum can seals. The method employs coprecipitation with chromophore ions ( $\text{Co}^{2+}$ ) and subsequent calcination, enabling the production of pigments with distinct shades by varying the proportion of the coloring ion in the aluminate matrix.

## 2. Materials and Methods

### 2.1. Materials

Discarded aluminum can seals were collected from can collectors in Guarapuava, Paraná, Brazil. The hydrochloric acid (HCl) utilized in this study was sourced from the brand Synth, the cobalt chloride ( $\text{CoCl}_2 \cdot \text{H}_2\text{O}$ ) was obtained from the brand Dinâmica (São Paulo, Brazil), and the sodium hydroxide (NaOH) was acquired from the brand Neon (Suzano, Brazil).

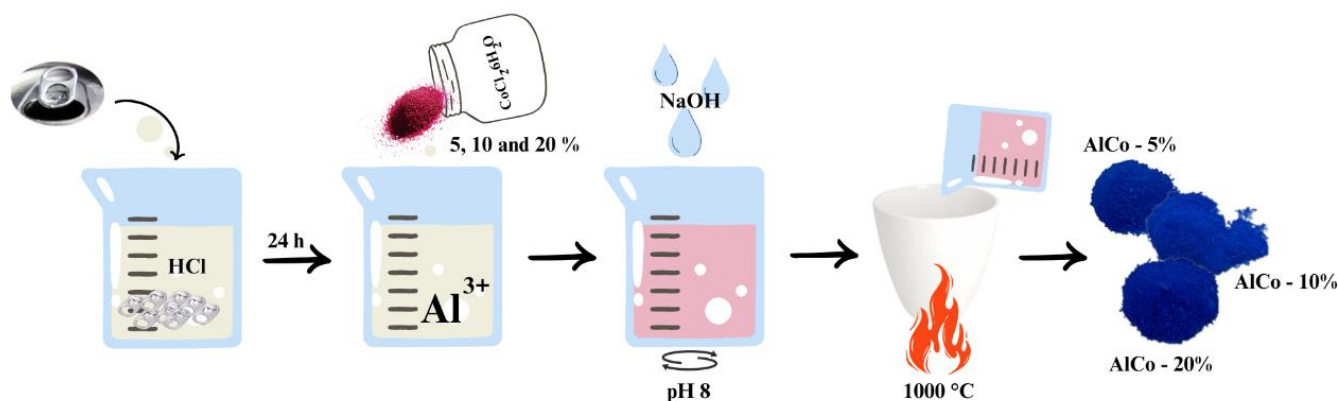
### 2.2. Methods

The aluminate synthesis process, illustrated in Figure 1, initiates with the acid digestion of discarded aluminum can seals utilizing hydrochloric acid (HCl) in an aqueous solution at a concentration of 1.1 mol/L. In this first step, approximately 1 g of aluminum is introduced into 100 milliliters of the hydrochloric acid solution. Acid digestion is a crucial phase that facilitates the dissolution of aluminum, allowing for the extraction of aluminum ions ( $\text{Al}^{3+}$ ) into the solution. This process is conducted over a period of 24 h to ensure that the reaction medium stabilizes and that the aluminum is fully converted into soluble ions.

Following the completion of the acid digestion, the next step involves the careful addition of cobalt (II) chloride hexahydrate ( $\text{CoCl}_2 \cdot 6\text{H}_2\text{O}$ ) to the solution now rich in  $\text{Al}^{3+}$  ions. This addition is pivotal as it sets the stage for the subsequent coprecipitation process. To achieve optimal conditions for coprecipitation, sodium hydroxide (NaOH) in aqueous form, with a concentration of 2 mol/L, is gradually dripped into the solution. The pH is meticulously monitored and maintained at approximately 8 during this addition. Continuous stirring is employed throughout this step to ensure thorough mixing and homogeneity of the reaction medium, which aids in the formation of a uniform precipitate. Once the desired pH is reached, a precipitate of aluminum and cobalt hydroxides forms. This precipitate is then subjected to a calcination process, which involves heating it to 1000 °C. The calcination is performed for 1 h, with a controlled heating ramp of 10 °C per minute. This thermal treatment is essential for the transformation of the hydroxides into stable aluminate compounds, enhancing their structural integrity and performance characteristics.

After the calcination process is complete, the resulting pigments are not yet ready for application, as they contain residual sodium chloride (NaCl), a coproduct from the coprecipitation phase. To eliminate this unwanted byproduct, the pigments undergo a washing procedure with hot water. This washing step is critical to removing any remaining NaCl, ensuring that the final product is pure and suitable for its intended applications.

The amount of  $\text{Co}^{2+}$  in the prepared samples was 5, 10, and 20% (*w/w*), and the samples were labeled CoAl-5%, CoAl-10%, and CoAl-20%, respectively.



**Figure 1.** Scheme of cobalt aluminate synthesis, highlighting the main steps.

### 2.3. Characterization Techniques

The samples were characterized by X-ray diffraction (XRD), carried out in an Empyrean model D2 Phaser diffractometer from Bruker (Billerica, MA, US.), equipped with a copper cathode ( $\lambda = 1.5418 \text{ \AA}$ ), operated at 30 kV with a current of 10 mA, and with a working window between  $10^\circ$  and  $80^\circ$  ( $2\theta$ ), scanned with a step of  $0.02^\circ/\text{s}$ . A scanning electron microscope, the Hitachi SU8020 SEM (Tokyo, Japan), equipped with an EDX 4505A–6UUS-SN (ang. energy dispersive X-ray) spectrometer, with a resolution of 134 eV (Thermo Scientific, Waltham, MA, USA), was used to observe the sample morphology and elemental composition.

The visible spectra were obtained using the Ocean Optics spectrophotometer (USB 2000), equipped with an optical fiber, tungsten–halogen source, and silicon (350–720 nm) and germanium (720–1050 nm) detectors. The band gap was determined using the Kubelka–Munk method [17], with reflectance measured using the Agilent Cary 5000 UV–vis–NIR spectrometer (Santa Clara, CA, USA). The optical reflectance of the pigment powder was measured using a UV–vis–NIR spectrophotometer (Perkin Elmer Lambda 950, Waltham, MA, USA). As a baseline standard,  $\text{BaSO}_4$  was used to measure the optical properties of the samples between 300 and 2500 nm. The NIR solar reflectance ( $R^*$ ) of the pigments in the wavelength range of 750–2500 nm was calculated using the following Equation (1):

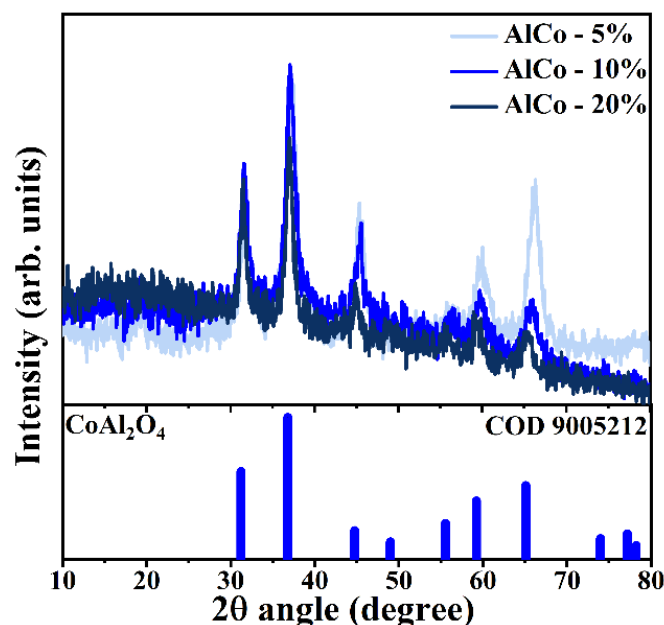
$$R_s = \frac{I_R}{I_0} = \frac{\int_0^\infty r_\lambda i_{\lambda,i} d\lambda}{\int_0^\infty i_{\lambda,i} d\lambda} \quad (1)$$

where  $r(\lambda)$  is the spectral reflectance obtained from the experimental study, and  $i(\lambda)$  is the spectral irradiance obtained from the standard ASTM G173–03 [18] reference spectra ( $\text{W}\cdot\text{m}^{-2}\cdot\text{nm}^{-1}$ ).

## 3. Results

### 3.1. Structural Investigation by X-ray Diffraction (XRD)

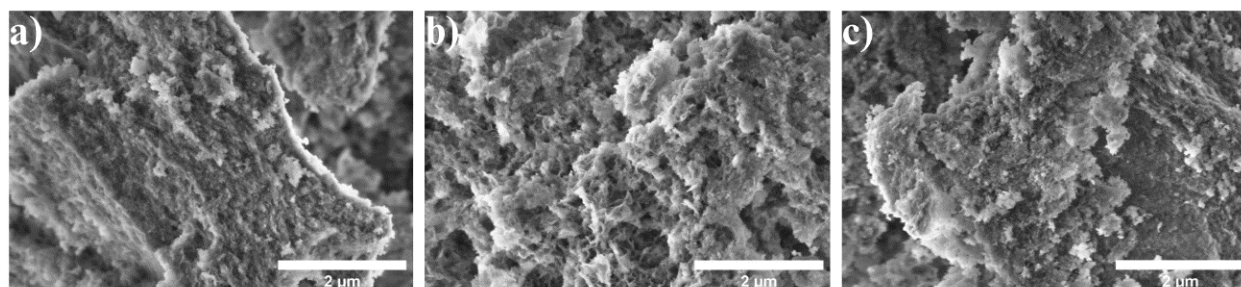
Figure 2 presents the X-ray diffraction (XRD) patterns of the synthesized samples, depicted in various shades of blue. These diffractograms were indexed using data from the Crystallography Open Database (COD), specifically using crystallographic chart 9005212, which corresponds to spinel cobalt aluminate ( $\text{CoAl}_2\text{O}_4$ ). This compound is characterized by a cubic crystalline structure in which  $\text{Co}^{2+}$  ions occupy tetrahedral sites, while  $\text{Al}^{3+}$  ions are situated in octahedral positions [19]. Analyzing the crystallographic profile derived from the diffractograms, the unit cell parameters were calculated, yielding a value of  $a = 0.801 \text{ nm}$ . In spinel systems, the unit cell is defined by the relationship  $a = b = c$ , with theoretical values typically ranging from approximately 0.80 nm to 0.81 nm [18]. The background noise observed in the diffractograms indicates the presence of an amorphous phase, which is likely associated with the formation of transition alumina due to the specific conditions under which the synthesis was conducted [20].



**Figure 2.** Diffractograms of the samples CoAl-5%, CoAl-10%, and CoAl-20% indexed according to the COD 9005212 standard for CoAl<sub>2</sub>O<sub>4</sub>.

### 3.2. Morphology by Scanning Electron Microscopy (SEM)

The morphology observed in the micrographs (Figure 3) reveals the presence of agglomerates with rough, irregular surfaces. These agglomerates appear to be composed of small sheets or platelets that are distributed unevenly across the sample's surface. The formation of such agglomerates can be attributed to the synthesis conditions, particularly the high temperatures used during the process. As reported in previous studies, agglomeration tends to increase at elevated temperatures due to the rise in surface energy, which drives particle interactions and clustering [21,22]. At higher temperatures, the kinetic energy of the particles within the material also increases significantly, contributing to enhanced mobility. This heightened particle mobility facilitates the diffusion and migration of smaller particles toward larger ones, a phenomenon known as Ostwald ripening. Ostwald ripening is a key mechanism by which larger particles grow at the expense of smaller ones, leading to the eventual formation of agglomerates. As the particles move and coalesce, the material's surface becomes more irregular and coarser, which is clearly visible in the observed micrographs [21]. Furthermore, the agglomeration process may also be influenced by the synthesis method and the nature of the precursor materials used. In this context, the increased temperature likely facilitates the sintering of particles, a process where adjacent particles adhere to each other, further reinforcing the formation of agglomerates. This sintering effect can result in the merging of smaller particles into larger structures, which ultimately leads to the rough, sheet-like morphology observed. The presence of these agglomerates can impact the material's final properties, such as its surface area, porosity, and overall structural integrity, which may be relevant for its intended applications in ceramics, pigments, or catalysis [22]. In addition to these effects, the extent of agglomeration can also depend on the cooling rate following high-temperature synthesis. Rapid cooling may trap the particles in a more agglomerated state, while slow cooling could allow for some degree of particle separation or rearrangement.



**Figure 3.** SEM micrographs of samples: (a) AlCo-5%, (b) AlCo-10%, and (c) AlCo-20%.

### 3.3. Elemental Composition by Energy-Dispersive X-ray Spectroscopy (EDX)

Table 1 presents the estimated elemental composition of the samples with the total amount of the elements in the samples. Sodium and chlorine were detected, but the low percentage of chlorine (Cl) makes it difficult to attribute NaCl exclusively as a byproduct of the reaction. The similar cobalt concentrations in the AlCo-10% and AlCo-20% samples may be due to the synthesis conditions, which limit cobalt incorporation into the structure. Unlike other studies that use fuels in the synthesis, this research study does not, which could explain the lower cobalt levels observed [20]. However, according to EDX performed in conjunction with SEM, the presence of cobalt is homogeneous across the entire surface of the samples. The approximate values of the Co/Al ratio were 0.1, 0.25, and 0.31 for AlCo-5%, AlCo-10%, and AlCo-20%, respectively. The expected ratio for spinel  $\text{CoAl}_2\text{O}_4$  is 0.5, when it is synthesized stoichiometrically. In the case of this study, the percentage of cobalt added is lower than ideal, but the formation of the compound occurs satisfactorily, preserving the intense blue color.

**Table 1.** Elemental composition of samples determined by EDX.

Sample	Elements (at. %)				
	Al	O	Co	Na	Cl
AlCo-5%	32.5	61.3	3.2	2.3	0.7
AlCo-10%	32.2	57.1	8.0	2.0	0.7
AlCo-20%	30.7	58.3	9.5	1.4	0.1

### 3.4. Optical and Colorimetric Characteristics (Vis and Colorimetry)

Figure 4 shows the absorbance spectra of the samples in the visible region, highlighting a prominent triplet at approximately 548, 585, and 627 nm. This feature is attributed to the  $\text{Co}^{2+}$  ion transition  ${}^4\text{A}_2(\text{F}) \rightarrow {}^4\text{T}_1(\text{P})$ , which is spin-allowed in tetrahedral geometries exhibiting Jahn–Teller distortion, contributing to its blue coloration [23]. Additionally, a minor band around 482 nm is observed, likely resulting from the forbidden spin transitions of the tetrahedral/octahedral  $\text{Co}^{2+}$  cations; however, this may also indicate ligand-to-metal charge transfer (LMCT) transitions [23].

The reflectance spectra (Figure 5a) confirm the presence of bands associated with the transitions of the  $\text{Co}^{2+}$  ions. The band gap, calculated using the Kubelka–Munk method (Figure 5b), exhibited minimal variation with changes in the cobalt concentration within the sample. The valence band is primarily composed of the 3d orbitals of cobalt atoms and the 2p orbitals of oxygen atoms. In contrast, the conduction band is mainly formed by the 3d orbitals of cobalt atoms and the 3p orbitals of aluminum atoms. The electronic states near the Fermi level are mainly dominated by the 3d orbitals of cobalt atoms, which significantly affect the optical properties of  $\text{CoAl}_2\text{O}_4$  [24]. The similarity in cobalt content for the samples accounts for the comparable bandgap values observed.

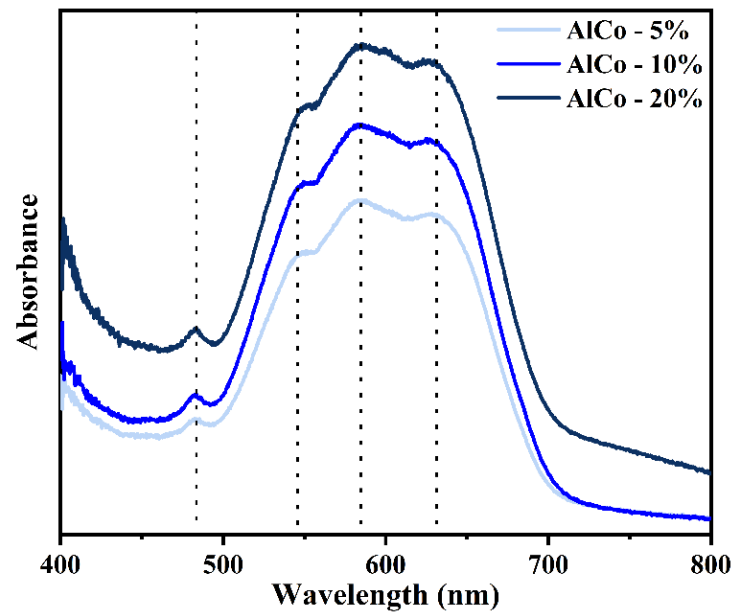


Figure 4. Absorbance spectra of AlCo-5%, AlCo-10%, and AlCo-20% samples in the visible region.

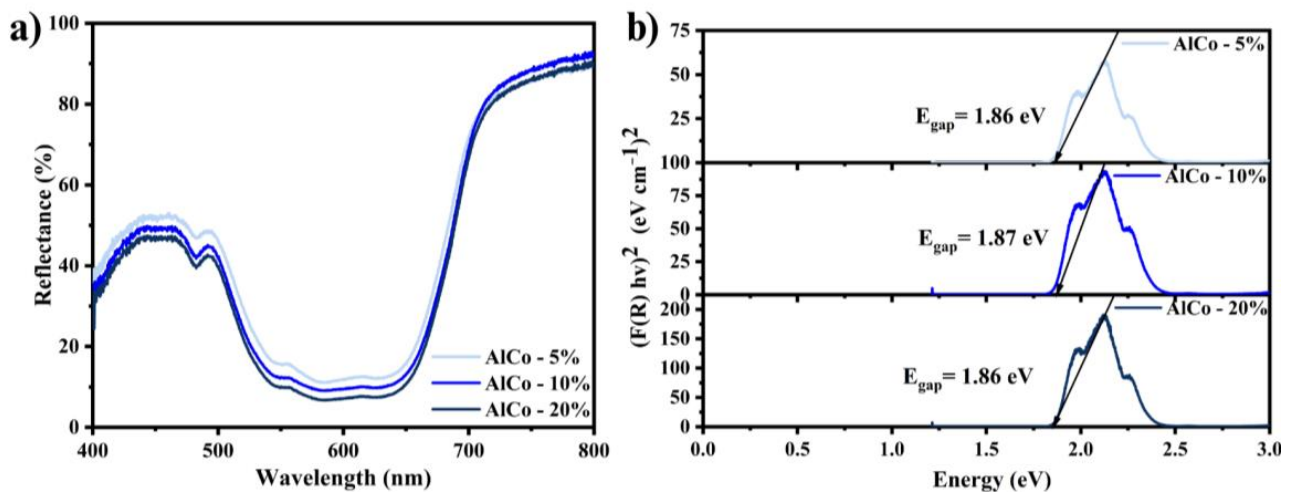





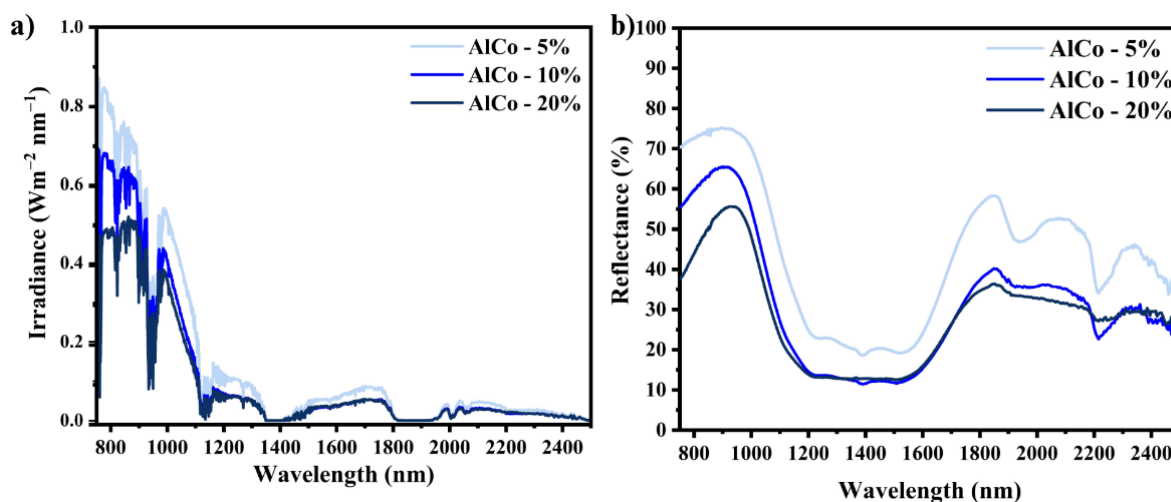
Figure 5. (a) The reflectance spectra of the cobalt aluminates and (b) the optical band gap calculated using the Kubelka–Munk method for the cobalt aluminates (AlCo-5%, AlCo-10%, and AlCo-20%).

The colorimetric parameters are presented in Table 2, illustrating a reduction in luminosity concomitant with an increase in cobalt ion concentration. The chroma ( $C^*$ ) parameter is an indicator of color saturation level, quantifiable as the distance from the color point to the  $L^*$  axis. The chroma value of a color can be calculated from the color coordinates using the Pythagorean theorem:  $C^* = \sqrt{a^{*2} + b^{*2}}$ . Highly saturated colors are represented by points situated further from the luminosity axis, whereas light colors with low saturation are located near the  $L^*$  axis. Achromatic colors, encompassing the spectrum from black through gray to white, exhibit a chroma value of zero, with their corresponding color points aligned along the  $L^*$  axis. In the paint industry, a commonly accepted criterion is that achromatic colors possess a  $C^*$  below 10, thus defining chromatic colors as those with  $C^*$  values exceeding 10 [25,26].

**Table 2.** Colorimetric parameters are determined by Colorimetry in the CIEL\*a\*b\* color space.

Sample	Colorimetric Parameters				Photo
	L*	a*	b*	C*	
AlCo-5%	34.57	−0.97	−34.77	34.79	
AlCo-10%	19.26	14.73	−43.59	46.01	
AlCo-20%	5.86	−2.08	−41.00	41.05	

The near-infrared (NIR) reflectance spectra of the powder pigments are presented in Figure 6, corresponding to the NIR reflectance spectra calibrated according to the measurement standard JG/T235-2014. In this standard, the spectral reflectance is adjusted by multiplying it by the normalized solar hemispheric irradiance  $i(\lambda)$ . The reflectance values recorded were 34% for AlCo-5%, 41.3% for AlCo-10%, and 54% for the AlCo-20% sample. These results indicate the significant impact of the chromophore ion concentration on the reflectance characteristics.

**Figure 6.** NIR solar reflectance spectra for the cobalt aluminates (AlCo-5%, AlCo-10%, and AlCo-20%): (a) irradiance spectra and (b) reflectance spectra.

#### 4. Discussion

This study presents an eco-friendly alternative for the recycling of metallic aluminum aiming at obtaining cobalt aluminates using acid digestion, followed by coprecipitation with different concentrations of cobalt chromophore ions and subsequent calcination at 1000 °C. Structural analyses demonstrate that the crystallographic arrangement of the synthesized samples aligns with the crystallographic pattern of cobalt aluminate, as referenced in crystallographic chart COD 9005212. This spinel phase indicates the presence of trivalent aluminum ions (Al<sup>3+</sup>) occupying octahedral sites and divalent cobalt ions (Co<sup>2+</sup>) situated in the tetrahedral sites. The reflectance spectra reveal a low-intensity band at 482 nm,

typically associated with forbidden spin transitions of the tetrahedral/octahedral  $\text{Co}^{2+}$  cations. This result suggests a degree of inversion within the spinel structure, wherein  $\text{Co}^{2+}$  ions may also occupy octahedral sites, potentially leading to a color shift toward green [7]. The hue observed in the samples, classified as “cobalt blue”, suggests that the extent of inversion in the spinel structure is minimal. Furthermore, the morphology of the agglomerates, primarily influenced by the calcination temperature of  $1000\text{ }^{\circ}\text{C}$ , plays a crucial role in determining color and reflectivity. The agglomeration of particles can reduce light scattering capabilities, resulting in darker coloration, a trend that intensifies with the increasing cobalt ion concentration in the samples. In cobalt-based pigments, cobalt ions selectively absorb light in the red and green regions of the visible light spectrum. When white light interacts with cobalt-containing materials, these ions absorb red and green photons, promoting electron transitions to higher energy levels. Conversely, blue photons experience less absorption due to the specific characteristics of the electronic orbitals associated with cobalt ions. Consequently, when a photon interacts with a cobalt ion, absorption occurs only if its energy aligns with the energy gap between the cobalt d-orbital levels. Thus, blue light is predominantly reflected, leading to the perception of blue coloration, which becomes more pronounced with increased cobalt content [8]. In contrast, reduced concentrations of cobalt ions enhance the reflectivity of the materials in both the visible and near-infrared (NIR) regions, as lower chromophore ion content results in diminished light absorption, thereby facilitating greater radiation reflection. The literature indicates reflectance values (R%) of  $\sim 50\%$  in the NIR region for cobalt aluminate [7,9], indicating that the application of pigments obtained by recycling aluminum can seals can be applied as functional pigments, highlighting their reflective capacity.

## 5. Conclusions

This study provides valuable insights into the synthesis of cobalt aluminate pigments from recycled aluminum can seals, highlighting an innovative and sustainable method for producing near-infrared (NIR) reflective blue pigments. By employing acid digestion and coprecipitation techniques with varying concentrations of cobalt chromophore ions, the resulting pigments exhibit NIR reflectance ranging from 34% to 54%. Of particular note, the sample with a 20% cobalt content achieved an R% value of 54% in the NIR region, surpassing the expected reflectance of undoped cobalt aluminates. This enhancement in NIR reflectance demonstrates the effectiveness of the doping strategy in optimizing the material’s optical properties.

Structural characterization through X-ray diffraction confirmed the successful formation of the spinel phase, consistent with the crystallographic pattern of cobalt aluminate, verifying the proper incorporation of aluminum and cobalt ions within the crystal lattice. The spinel structure plays a critical role in ensuring both the stability and color intensity of the pigments. The optical properties further underscore the high quality of the pigments, with their distinct blue coloration resulting from selective absorption of red and green wavelengths and the dominant reflection of blue light, which enhances the pigment’s visual hue. The intense chromatic colors, characterized by chroma ( $C^*$ ) values exceeding 30%, demonstrate the material’s ability to produce vibrant, saturated colors, making them ideal for esthetic and functional applications.

The morphological analysis indicates that the rough, sheet-like structure of the pigments, influenced by calcination temperature, plays a pivotal role in enhancing their light-scattering capabilities, thereby amplifying their color intensity. This relationship between morphology and optical performance highlights the importance of controlled synthesis conditions in achieving optimal pigment characteristics. The study also illustrates how varying synthesis parameters, such as cobalt ion concentration and calcination temperature, can be used to fine-tune the pigment’s properties for specific applications.

The eco-friendly nature of these pigments, derived from recycled materials, positions them as highly suitable candidates for use in energy-efficient coatings. The significant NIR reflectance values suggest that these pigments can effectively reduce heat gain on



surfaces such as roofs, walls, and vehicles, contributing to reduced energy consumption in cooling systems. This feature is particularly relevant for applications in climate control and sustainable building design, where heat-reflective coatings can play a key role in enhancing energy efficiency. By reflecting a substantial portion of NIR radiation, these pigments help mitigate the urban heat island effect and improve thermal comfort in buildings without the need for intensive air conditioning.

In addition to their energy-saving potential, the recycling of aluminum can seals through this process aligns with the principles of a circular economy, reducing waste and promoting the sustainable use of resources. This method not only provides an efficient way to repurpose aluminum waste but also offers a scalable, low-cost approach to pigment production. The synthesis of cobalt aluminates from recycled materials represents a promising pathway for the development of eco-friendly pigments that serve both esthetic and functional purposes in a variety of industries, including construction, automotive, and consumer goods.

In conclusion, the findings of this study highlight the viability and practicality of producing cobalt aluminate pigments via the recycling of aluminum can seals. The demonstrated NIR reflectance, structural integrity, and vibrant coloration of these pigments make them suitable for a wide range of applications, particularly in energy-efficient coatings. Moreover, the integration of recycled materials in the synthesis process not only supports environmental sustainability but also offers a cost-effective alternative to traditional pigment production methods. This work paves the way for further research into the development of advanced, sustainable materials that can contribute to energy conservation and environmental stewardship, reinforcing the importance of circular economy principles in modern industrial processes.

**Author Contributions:** Conceptualization, D.F.L.H., F.J.A. and C.B.; methodology, D.F.L.H. and J.d.O.P.; validation, J.d.O.P. and D.F.L.H.; formal analysis, D.F.L.H. and J.d.O.P.; investigation, D.F.L.H. and J.d.O.P.; resources, C.B. and F.J.A.; writing—original draft preparation, D.F.L.H.; writing—review and editing, D.F.L.H., F.J.A., P.U. and C.B.; visualization, D.F.L.H. and C.B.; supervision, F.J.A. and C.B.; project administration, F.J.A. and C.B.; funding acquisition, F.J.A. and C.B. All authors have read and agreed to the published version of the manuscript.

**Funding:** D.F.L.H. and J.d.O.P. appreciate the Coordenação de Aperfeiçoamento de Pessoal de Nível Superior/Brasil (CAPES)—Finance Code 001—graduate scholarship and the FNRS for mobility grant (2021/V6/5/003–JG/MF–726). C.B. is a research associate of FRS-FNRS, Belgium. C.B., and thanks the Belgian Fund for Scientific Research under the FRFC contract EQP 40002995 (PHOTOFUN). F.J.A. is thankful for a CNPq Productivity grant (308625/2019-6) and the grants CNPq–427127/2018-1 and Fundação Araucária–CBPA-001/2016.

**Institutional Review Board Statement:** Not applicable.

**Informed Consent Statement:** Not applicable.

**Data Availability Statement:** The original contributions presented in the study are included in the article, further inquiries can be directed to the corresponding authors.

**Acknowledgments:** The authors are grateful to UNICENTRO and UMons.

**Conflicts of Interest:** The authors declare no conflicts of interest.

## References

1. Chen, Z.; Shi, E.; Li, W.; Zheng, Y.; Zhong, W. Hydrothermal Synthesis and Optical Property of Nano-Sized  $\text{CoAl}_2\text{O}_4$  Pigment. *Mater. Lett.* **2002**, *55*, 281–284. [[CrossRef](#)]
2. Zou, J.; Chen, Y.; Zhang, P. Influence of crystallite size on color properties and NIR reflectance of  $\text{TiO}_2@ \text{NiTiO}_3$  inorganic pigments. *Ceram. Int.* **2021**, *47*, 12661–12666. [[CrossRef](#)]
3. Primo, J.d.O.; Borth, K.W.; Peron, D.C.; Teixeira, V.d.C.; Galante, D.; Bittencourt, C.; Anaissi, F.J. Synthesis of green cool pigments ( $\text{Co}_x\text{Zn}_{1-x}\text{O}$ ) for application in NIR radiation reflectance. *J. Alloys Compd.* **2019**, *780*, 17–24. [[CrossRef](#)]
4. Gates, D.M. Solar Radiation. In *Biophysical Ecology*; Gates, D.M., Ed.; Springer: New York, NY, USA, 1980; pp. 96–147. [[CrossRef](#)]

5. Stuart-Fox, D.; Newton, E.; Mulder, R.A.; D'Alba, L.; Shawkey, M.D.; Igic, B. The microstructure of white feathers predicts their visible and near-infrared reflectance properties. *PLoS ONE* **2018**, *13*, e0199129. [[CrossRef](#)] [[PubMed](#)]
6. Smith, A.E.; Comstock, M.C.; Subramanian, M.A. Spectral properties of the UV absorbing and near-IR reflecting blue pigment,  $\text{YIn}_{1-x}\text{Mn}_x\text{O}_3$ . *Dyes Pigment.* **2016**, *133*, 214–221. [[CrossRef](#)]
7. Sangeetha, S.; Basha, R.; Sreeram, K.J.; Sangilimuthu, S.N.; Nair, B.U. Functional pigments from chromium(III) oxide nanoparticles. *Dyes Pigment.* **2012**, *94*, 548–552. [[CrossRef](#)]
8. Levinson, R.; Berdahl, P.; Akbari, H.; Miller, W.; Joedicke, I.; Reilly, J.; Suzuki, Y.; Vondran, M. Methods of creating solar-reflective nonwhite surfaces and their application to residential roofing materials. *Sol. Energy Mater. Sol. Cells* **2007**, *91*, 304–314. [[CrossRef](#)]
9. Levinson, R.; Berdahl, P.; Akbari, H. Solar spectral optical properties of pigments—Part I: Model for deriving scattering and absorption coefficients from transmittance and reflectance measurements. *Sol. Energy Mater. Sol. Cells* **2005**, *89*, 319–349. [[CrossRef](#)]
10. Raj, A.K.V.; Rao, P.P.; Divya, S.; Ajuthara, T.R. Terbium doped  $\text{Sr}_2\text{MO}_4$  [M = Sn and Zr] yellow pigments with high infrared reflectance for energy saving applications. *Powder Technol.* **2017**, *311*, 52–58. [[CrossRef](#)]
11. Chen, J.; Zhang, J.; Hu, M.; Zheng, Z.; Wang, K.; Li, X. Preparation of Ni/graphene hydrophobic composite coating with micro-nano binary structure by poly-dopamine modification. *Surf. Coat. Technol.* **2018**, *353*, 1–7. [[CrossRef](#)]
12. Takebayashi, H.; Moriyama, M. Surface heat budget on green roof and high reflection roof for mitigation of urban heat island. *Build. Environ.* **2007**, *42*, 2971–2979. [[CrossRef](#)]
13. Gao, Q.; Wu, X.; Fan, Y.; Meng, Q. Color performance and near infrared reflectance property of novel yellow pigment based on  $\text{Fe}_2\text{TiO}_5$  nanorods decorated mica composites. *Dyes Pigment.* **2017**, *146*, 537–542. [[CrossRef](#)]
14. He, R.; Hocking, R.K.; Tsuzuki, T. Co-doped ZnO nanopowders: Location of cobalt and reduction in photocatalytic activity. *Mater. Chem. Phys.* **2012**, *132*, 1035–1040. [[CrossRef](#)]
15. Ke, S.; Pan, Z.; Wang, Y.; Ning, C.; Zheng, S.; Huang, J. Effect of mechanical activation on solid-state synthesis process of neodymium disilicate ceramic pigment. *Dyes Pigment.* **2017**, *145*, 160–167. [[CrossRef](#)]
16. Fu, J.; Ren, X.; Yan, S.; Gong, Y.; Tan, Y.; Liang, K.; Du, R.; Xing, X.; Mo, G.; Chen, Z.; et al. Synthesis and structural characterization of ZnO doped with Co. *J. Alloys Compd.* **2013**, *558*, 212–221. [[CrossRef](#)]
17. Morales-Marín, A.; Ayastuy, J.L.; Iriarte-Velasco, U.; Gutiérrez-Ortiz, M.A. Nickel aluminate spinel-derived catalysts for the aqueous phase reforming of glycerol: Effect of reduction temperature. *Appl. Catal. B Environ.* **2019**, *244*, 931–945. [[CrossRef](#)]
18. CIE, C. Recommendations on uniform color spaces, color difference equations, psychometric color terms. *CIE Publ.* **1978**, *15*, 9–12.
19. Liu, Y.; Jia, L.; Hou, B.; Sun, D.; Li, D. Cobalt aluminate-modified alumina as a carrier for cobalt in Fischer–Tropsch synthesis. *Appl. Catal. A Gen.* **2017**, *530*, 30–36. [[CrossRef](#)]
20. Deraz, N.M. Formation and Characterization of Cobalt Aluminate Nano-Particles. *Int. J. Electrochem. Sci.* **2013**, *8*, 4036–4046. [[CrossRef](#)]
21. Podder, M.; Ahmed, M.F.; Moni, M.R.; Rahman, M.L.; Biswas, B.; Sharmin, N. Effect of metal ions on structural, morphological and optical properties of nano-crystallite spinel cobalt-aluminate ( $\text{CoAl}_2\text{O}_4$ ). *Arab. J. Chem.* **2023**, *16*, 104700. [[CrossRef](#)]
22. Bardaoui, A.; Dhifallah, I.; Daoudi, M.; Aouini, S.; Amlouk, M.; Chtourou, R. Exploring the impact of annealing temperature on morphological, structural, vibrational and electron paramagnetic resonance properties of starch-mediated spinel  $\text{CoAl}_2\text{O}_4$ : Experimental and DFT study. *J. Solid State Chem.* **2024**, *335*, 124732. [[CrossRef](#)]
23. Gingasu, D.; Mindru, I.; Culita, D.C.; Marinescu, G.; Somacescu, S.; Ianculescu, A.; Surdu, V.-A.; Preda, S.; Oprea, O.; Vasile, B.S. Mentha piperita-mediated synthesis of cobalt aluminate nanoparticles and their photocatalytic activity. *J. Mater. Sci. Mater. Electron.* **2021**, *32*, 11220–11231. [[CrossRef](#)]
24. He, Y.; Cao, Y.; Liao, H.; Wang, J.A. Preparation of porous cobalt aluminate and its chromogenic mechanism. *Powder Technol.* **2018**, *324*, 95–101. [[CrossRef](#)]
25. Beetsma, J. *The CIELAB System—The Method to Specify Colors of Coatings*; Ultrus Prospector Knowledge Center: Overland Park, KA, USA, 2024.
26. Mahy, M.; Van Eycken, L.; Oosterlinck, A. Evaluation of Uniform Color Spaces Developed after the Adoption of CIELAB and CIELUV. *Color. Res. Appl.* **1994**, *19*, 105–121. [[CrossRef](#)]

**Disclaimer/Publisher's Note:** The statements, opinions and data contained in all publications are solely those of the individual author(s) and contributor(s) and not of MDPI and/or the editor(s). MDPI and/or the editor(s) disclaim responsibility for any injury to people or property resulting from any ideas, methods, instructions or products referred to in the content.